Progress In Electromagnetics Research B, Vol. 29, 43–62, 2011

THE RENORMALIZATION GROUP THEORY COMBINED TO THE MS-GEC METHOD TO STUDY ACTIVE FRACTAL STRUCTURES WITH INCORPORATED PIN DIODES

S. Mili, C. Larbi Aguili, and T. Aguili

SysCom Laboratory
National Engineering School of Tunis
BP. 37 Le Belvedere 1002, Tunis, Tunisia

Abstract—The renormalization group theory (RGT) is used in this paper to develop an extension of the multi-scale approach (MS-GEC), previously developed by the authors, in order to enable the study of fractal structures at infinite iterations. In this work, we focused on active fractal structures with incorporated PIN diodes but the developed concept can be applied to a wide variety of fractals. The MS-GEC method deals with fractal-shaped objects as a set of scale levels. The processing is done gradually, one scale at each step, from the lowest scale till the highest one. To compute the input impedance of fractal-shaped structures using the MS-GEC method, we demonstrated that the input impedance of any scale level is generated from the input impedance of the previous scale level. When the iteration of fractal tends toward infinity, the structure contains an unknown number of levels. Since the atomic level cannot be defined, a critical point is reached limiting then the scope of the MS-GEC and of the existing classical methods. Based on RGT concepts, if the relation between the input impedances of two consecutive levels can be rewritten independently of the critical parameter (which is in our case the scale level), a transformation called "renormalization group" is generated. Consequently, the input impedance of the infinite active fractal structure approaches the fixed point of the defined transformation independently of the system details at the atomic level. The MS-GEC method combined to the RGT is a very powerful technique since it profits from the advantages (rapidity and reduced memory requirements) of the MS-GEC method and from the ability of the RGT to solve problems at their critical point.

Received 31 January 2011, Accepted 11 March 2011, Scheduled 15 March 2011
Corresponding author: Sonia Mili (sonia.mili.sayah@gmail.com).

1. INTRODUCTION

Due to their self-similarity and infinite complexities, fractal geometries [1] allow for small, multiband and broadband structures design [2–4]. Moreover, static behavior is no longer preferred and active structures have been researched to have tunable characteristics under the control of either semiconductor devices, or by utilizing ferrite as a substrate, or by incorporating PIN diodes, etc. [5–7]. The study of such active fractal objects at higher iterations requires very long solution time and important memory resources. At infinite iteration, the fractal structure is one of the toughest problems to deal with. Indeed, classical methods (MoM, FEM, TLM, etc.) are unable to study such structures since they cannot manipulate their infinite character. In a previous work [8], the authors have described the MS-GEC method which is proved so fruitful in gaining time and memory resources while allowing an accurate electromagnetic study of fractal-shaped structures. However, at infinite iterations of fractals, the MS-GEC reaches its limits since the microscopic level is no longer known and thus the starting elementary pattern cannot be neither defined nor studied. A critical point is reached and one wishes to remove such infinite character from the theory. To circumvent such difficulty, the MS-GEC method has been extended in this paper, using the renormalization group theory (RGT) [9–15].

To describe conveniently the RGT, we mention Wilson's own assessment of his achievement [10]: "This is the most exciting aspect of the renormalization group, the part of the theory that makes it possible to solve problems which are unreachable". As a result, thanks to the RGT, although the elementary scale level remains unknown, the infinite fractal structure can be investigated.

Using the MS-GEC method [8], the input impedance Z_{k_l} of any scale level k_l is generated from the input impedance Z_{k_l+1} of the previous scale level $(k_l + 1)$. This expression is the same for all scale levels but differs by the level dimensions. The main idea of the RGT is to rewrite the expression relating Z_{k_l} and Z_{k_l+1} in a dimensionless form; i.e., independently of the scale level k_l. The obtained expression is called transformation group or more precisely, "renormalization group". When the iteration of fractal increases, the input impedance of the fractal structure approaches the fixed point of the defined renormalization group. Therefore, the fixed point is the input impedance of the infinite fractal structure.

This paper is organized as follows: Section 2 provides an overview of the MS-GEC method where the relation between two consecutive scale levels is defined. In Section 3, the renormalization group theory is

introduced and then used to generate the renormalization group. The fixed point computation and validation are detailed in Section 4. The advantages of the developed method are described in Section 5.

2. OVERVIEW OF THE MS-GEC METHOD

The MS-GEC method [8] is a multi-scale (MS) approach combined to the generalized equivalent circuit (GEC) modeling [16–18]. Its objective is to simplify the study of complex structures and especially fractal ones. In this paper, the MS-GEC method is applied to compute the input impedance of the fractal structure with incorporated PIN diodes depicted Fig. 1 considered at an infinite iteration k. It consists of perfect metallic strips with negligible thickness printed on a lossless dielectric and related by PIN diodes. The structure is located in the cross-section of a parallel-plates EMEM waveguide: two perfect electric boundaries to the top and the bottom, lateral conditions are magnetic. Lets a and b be respectively the width and the height of this waveguide.

The MS-GEC method has been applied in [8] to compute the input impedance of the considered fractal structure at the 2nd and

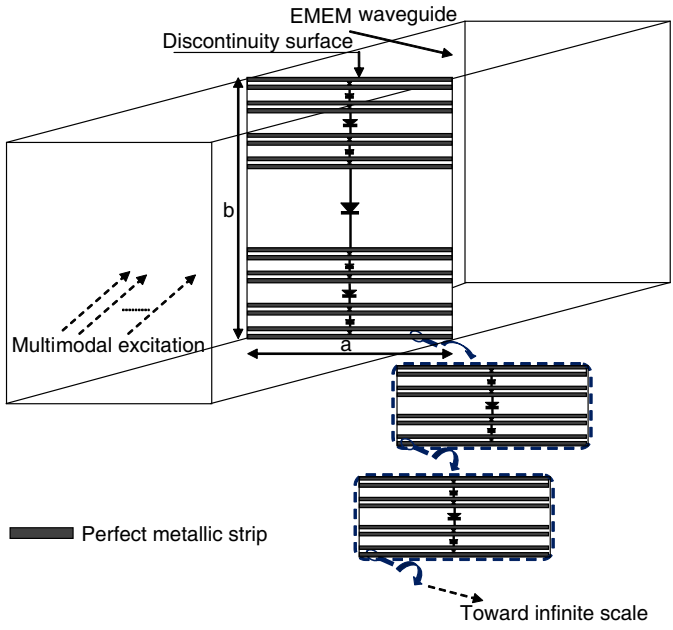

Figure 1. Fractal structure with incorporated PIN Diodes, located in the cross-section of an EMEM rectangular waveguide.

the 3rd stages of growth (called here iteration of fractal k) and then validated when compared to the Moment method. It was demonstrated that fractal objects can be treated as a set of scale levels: the input impedance of the whole structure can be computed gradually from the microscopic level to the macroscopic one. At each step, a scale level k_l is considered. The previous scale level $(k_l + 1)$ is integrated within the current scale level k_l using its equivalent input impedance operator $\hat{Z}_{k_l+1}$ which is derived from the corresponding input impedance matrix $[Z_{k_l+1}]$. Moreover, the PIN diode at scale level $k_l$is replaced by its equivalent surface impedance ZD_{k_l}.

At any scale level k_l, the structure to be considered is as drawn Fig. 2(a). Note that $(k_l = 0)$ refers to the highest level while $(k_l \to +\infty)$ denotes the microscopic level. α is called the scaling factor $(\alpha < 1)$: the scale level $(k_l + 1)$ is obtained by scaling the k_lth level by the factor α. Due to the structure symmetry with regard to the discontinuity surface, only the half of the generalized equivalent circuit (GEC) is needed [8]. The simplified GEC is depicted in Fig. 2(b).

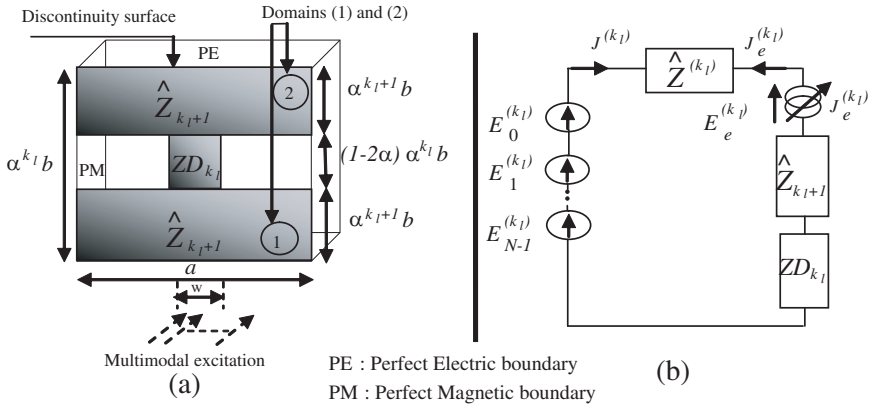

Figure 2. (a) Structure at the k_lth scale level where the previous level (k_l+1) is replaced by its input impedance operator $\hat{Z}_{k_l+1}$ and the PIN diode is replaced by its surface impedance ZD_{k_l}. (b) Its generalized equivalent circuit (GEC).

Lets $(f_{mn}^{(k_l)})$ be the local modal basis of the EMEM waveguide enclosing the considered scale level k_l. The excitation modal sources are $E_i^{(k_l)} = V_i^{(k_l)} f_i^{(k_l)}$ where $f_i^{(k_l)}$, $i \in \{0, 1, \ldots, N-1\}$ represent the active modes of scale level k_l and $V_i^{(k_l)}$ are their weighting coefficients. The impedance operator $\hat{Z}^{(k_l)}$ is expressed in (1) as a function of the

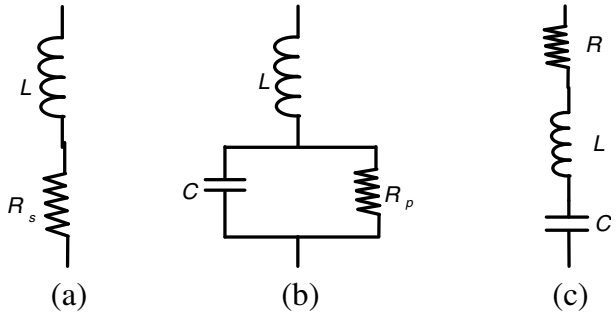

Figure 3. The PIN Diode. (a) Forward bias equivalent circuit. (b) Reverse bias equivalent circuit. (c) Reverse bias equivalent RLC circuit [8, 19].

higher-order modes $\langle f_{m,n}^{(k_l)}|$ and their modes' impedances $z_{m,n}^{(k_l)}$ [9].

$$\hat{Z}^{(k_l)} = \sum_{\substack{m,n \\ (m,n)\neq active}} \left|f_{m,n}^{(k_l)}\right\rangle z_{m,n}^{(k_l)} \left\langle f_{m,n}^{(k_l)}\right| \tag{1}$$

The problem's unknown $J_e^{(k_l)}$ is expressed as a series of known test functions $g_p^{(k_l)}$ weighted by unknown coefficients $x_p^{(k_l)}$.

$J_e^{(k_l)}$ exists on the $\hat{Z}_{k_l+1}$ domains and the diode domain and is zero on the lossless dielectric domain. The dual size of $J_e^{(k_l)}$,denoted $E_e^{(k_l)}$, is defined on the lossless dielectric domain. Thus, $J_e^{(k_l)}$ and $E_e^{(k_l)}$ verify the condition $\langle J_e^{(k_l)}, E_e^{(k_l)}\rangle = 0$.

One notes that the PIN diode is replaced by its surface impedance ZD_{k_l}. In fact, According to its ON/OFF state, each PIN diode can be modeled [8, 19] by one of the equivalent circuits depicted Fig. 3. In this paper, the values used for forward bias are $R = 5\,\Omega$ and $L = 0.4\,\text{nH}$. For reverse bias, a capacitance $C = 0.27\,\text{pF}$ is added. Consequently, the PIN diode at scale level k_l can be substituted by the surface impedance ZD_{k_l} of width w and height $d_{k_l} = (1-2\alpha)\alpha^{k_l} b$ using its intrinsic (R, L, C) characteristics [8] as expressed in (2).

$$ZD_{k_l} = \begin{cases} \frac{w}{d_{k_l}}\left(R + jL\omega\right) & : \text{forward bias} \\ \frac{w}{d_{k_l}}\left(R + jL\omega - \frac{j}{C\omega}\right) & : \text{reverse bias} \end{cases} \tag{2}$$

The impedance operator $\hat{Z}_{k_l+1}$ is a linear representation (3) of the input impedance matrix $[Z_{k_l+1}]$ of the previous scale level $(k_l + 1)$.

It is important to mention that $(f_i^{(k_l+1)})_{i\in[0,N-1]}$ are the active modes used as artificial excitation sources at the previous scale level (k_l+1) in order to compute its input impedance matrix.

$$\hat{Z}_{k_l+1} = \sum_{i=1}^{N}\sum_{j=1}^{N} \left|f_{i-1}^{(k_l+1)}\right\rangle \; Z_{k_l+1}(i,j) \; \left\langle f_{j-1}^{(k_l+1)}\right| \tag{3}$$

The generalized Ohm and Kirchhoff laws applied to the GEC depicted Fig. 2(b) lead to the equations system (4). The continuity of the current on the discontinuity surface is described by Equation (4a). Equation (4b) expresses the continuity of the field at the discontinuity surface.

$$\begin{cases} J^{(k_l)} = -J_e^{(k_l)} & \text{(4a)} \\ E_e^{(k_l)} = E_0^{(k_l)} + E_1^{(k_l)} + \ldots + E_{N-1}^{(k_l)} + \left(\hat{Z}^{(k_l)} + \hat{Z}_{k_l+1} + ZD_{k_l}\right) J_e^{(k_l)} & \text{(4b)} \end{cases} \tag{4}$$

A formal relation between sources (real and virtual) and their duals is then deduced (5).

$$\begin{pmatrix} J^{(k_l)} \\ E_e^{(k_l)} \end{pmatrix} = \begin{bmatrix} 0 & 0 & \ldots & 0 & -1 \\ 1 & 1 & \ldots & 1 & (\hat{Z}^{(k_l)} + \hat{Z}_{k_l+1} + ZD_{k_l}) \end{bmatrix} \begin{pmatrix} E_0^{(k_l)} \\ E_1^{(k_l)} \\ \vdots \\ E_{N-1}^{(k_l)} \\ J_e^{(k_l)} \end{pmatrix} \tag{5}$$

Next, we apply the Galerkin method to the equations system (4): Equations (4a) and (4b) are projected on the excitation modes $(f_i^{(k_l)})_{i\in[0,N-1]}$ and on the trial functions $(g_p^{(k_l)})_{p\in[1,Ne]}$ respectively. Therefore, the system (5) is rewritten as in (6).

$$\begin{pmatrix} \left[I^{(k_l)}\right] \\ [0] \end{pmatrix} = \begin{pmatrix} [0] & -\left[A^{(k_l)}\right] \\ \left[A^{(k_l)}\right]^T & \left[B^{(k_l)}\right] \end{pmatrix} \begin{pmatrix} \left[V^{(k_l)}\right] \\ \left[X^{(k_l)}\right] \end{pmatrix} \tag{6}$$

where:

$$\left[A^{(k_l)}\,(i,p)\right]_{\substack{i\in[0,N-1]\\ p\in[1,Ne]}} = \left[\left\langle f_i^{(k_l)}, g_p^{(k_l)}\right\rangle\right]$$

$$\left[B^{(k_l)}\,(p,q)\right]_{\substack{p\in[1,Ne]\\ q\in[1,Ne]}} = \left[\left\langle g_p^{(k_l)}, \left(\hat{Z}^{(k_l)} + \hat{Z}_{k_l+1} + ZD_{k_l}\right) g_q^{(k_l)}\right\rangle\right]$$

Equation (7) is the input impedance matrix $[Z_{k_l}]$ relative to the scale level k_l.

$$[Z_{k_l}] = \left(\frac{1}{2}\right)\left(\left[A^{(k_l)}\right]\;\left[B^{(k_l)}\right]^{-1}\;\left[A^{(k_l)}\right]^T\right)^{-1} \tag{7}$$

The input impedance matrix $[Z_{k_l}]$ varies with the dimensions of the considered scale level k_l which are related to the iteration of fractal k. When k tends toward infinity, the atomic level is unreachable. Consequently, the MS-GEC is unable to study infinite fractal structures. As a solution, the concepts of the renormalization group theory (RGT) have been exploited to suggest an extension of the MS-GEC method.

3. EXTENSION OF THE MS-GEC METHOD USING THE RENORMALISATION GROUP THEORY

To enlarge the scope of the MS-GEC method to infinite fractal structures, the concepts of the renormalization group theory have been employed.

3.1. Concepts of the Renormalization Group Theory (RGT)

The renormalization group theory describes an efficient manner to deal with problems involving many length scales [9–15]: the problem is treated gradually, one scale level at each step, from the atomic level to the macroscopic one. To compute the fluctuations on the larger scale, one needs to integrate out the fluctuations sequentially starting with those at the microscopic level and move gradually to the larger scale. According to K. G. Wilson [9, 10], the fluctuations can be safely incorporated into effective parameters without altering the real aspect of the theory. Moreover, one can start from any intermediate level with a physically appropriate parameter in place of the realistic one.

The main concept of the RGT is described as follows [9]: "Lets F_{k_l} be the functional describing the fluctuations at the scale level k_l. Since computation is done gradually, F_{k_l} is generated from the functional F_{k_l+1} describing the fluctuations on the previous level $(k_l + 1)$. If the relation between F_{k_l} and F_{k_l+1} is expressed in a dimensionless form, the generated transformation is called transformation group or more precisely "renormalization group". This latter is covariant since it does not reveal any characteristic scale. Consequently, at the larger length scale, the function F_{k_l} approaches the fixed point of the renormalization group independently of the system details at the microscopic level".

3.2. The MS-GEC Combined to the RGT: MS-RGT

Before using the RGT to extend the MS-GEC approach, one needs to verify if this latter performs computation similarly to RGT. In fact, since a fractal structure is obtained by an iterative process, the MS-GEC is reduced to a recursive algorithm as stated in Section 2 and

described in [8]: the problem is treated gradually from the lower scale level to the highest one. The fluctuation to which we are interested is the input impedance of the fractal structure at infinite scale. To compute it, we can start from any scale level k_l: its input impedance operator $\hat{Z}_{k_l}$ describes conveniently the details of the lower scales if the number of active modes used at each level is sufficiently enough [8].

It is clear that the MS-GEC performs computation as does the RGT. The next step is to determine an explicit relation between the input impedances of two consecutive scale levels. For that, we begin from the input impedance matrix $[Z_{k_l}]$ of scale level k_l (7).

$$\begin{aligned}
[Z_{k_l}] &= \left(\frac{1}{2}\right)\left(\left[A^{(k_l)}\right]\left[B^{(k_l)}\right]^{-1}\left[A^{(k_l)}\right]^T\right)^{-1} \\
&= \left(\frac{1}{2}\right)\left(\left[A^{(k_l)}\right]\left[\left\langle g_p^{(k_l)}, \hat{Z}^{(k_l)} g_q^{(k_l)}\right\rangle + \left\langle g_p^{(k_l)}, \hat{Z}_{k_l+1} g_q^{(k_l)}\right\rangle \right.\right. \\
&\quad \left.\left. + \left\langle g_p^{(k_l)}, ZD_{k_l} g_q^{(k_l)}\right\rangle\right]^{-1}\left[A^{(k_l)}\right]^T\right)^{-1} \\
\Rightarrow [Z_{k_l}] &= \left(\frac{1}{2}\right)\left(\left[A^{(k_l)}\right]\left[\left[B_1^{(k_l)}\right]+\left[B_2^{(k_l,k_l+1)}\right]+\left[B_{3D}^{(k_l)}\right]\right]^{-1}\left[A^{(k_l)}\right]^T\right)^{-1} \quad (8)
\end{aligned}$$

To extract the relation between $[Z_{k_l}]$ and $[Z_{k_l+1}]$, we need to do further calculations. For that, the modal basis $(f_{m,n}^{(k_l)})$, the excitation sources $(f_i^{(k_l)})_{i\in[0,N-1]}$ and the trial functions $(g_p^{(k_l)})$ used to study the scale level k_l (Fig. (2a)) are detailed in Appendix A.

3.2.1. Explicit Relation between $[Z_{k_l}]$ and $[Z_{k_l+1}]$

Using the excitation sources and the trial functions detailed in Appendix A, the matrix $[A^{(k_l)}]$ used in (8) is rewritten as in (9) where the matrix $[A]$ is constant, i.e., independent of the scale level k_l.

$$\left[A^{(k_l)}\right] = \sqrt{\alpha^{k_l}}\ [A] \quad (9)$$

As shown in (8), the matrix $[B^{(k_l)}]$ is the sum of three matrices $[B_1^{(k_l)}]$, $[B_2^{(k_l,k_l+1)}]$ and $[B_{3D}^{(k_l)}]$ where $[B_1^{(k_l)}]$ expresses the contribution of the higher-order modes of the k_lth scale level. $[B_2^{(k_l,k_l+1)}]$ is due to the impedance operator $\hat{Z}_{k_l+1}$ describing the previous level (k_l+1). $[B_{3D}^{(k_l)}]$ is due to the surface impedance ZD_{k_l} of the PIN diode at scale level k_l.

Detailed expression of $[B_1^{(k_l)}]$

$[B_1^{(k_l)}]$ is due to the higher-order modes $\{TE_{m,n}^{(k_l)}, TE_{m,0}^{(k_l)}, TM_{m,n}^{(k_l)}, TM_{\substack{0,n \\ n\neq n_{active}}}^{(k_l)}\}$ of scale level k_l (Appendix A). Therefore, it can be expressed by (10).

$$\left[B_1^{(k_l)}\right] = \left[B_{1\ m\neq 0\&n\neq 0}^{TE_{m,n}^{(k_l)}}\right] + \left[B_{1\ m\neq 0}^{TE_{m,0}^{(k_l)}}\right] + \left[B_{1\ m\neq 0\&n\neq 0}^{TM_{m,n}^{(k_l)}}\right] + \left[B_{1\ n\neq n_{active}}^{TM_{0,n}^{(k_l)}}\right] \quad (10)$$

A detailed calculation leads to Equation (11) where $[B_1^{TE_{m,n}}]$, $[B_1^{TE_{m,0}}]$, $[B_1^{TM}]$ are constant, i.e., independent of the scale level k_l.

$$\begin{aligned}\left[B_1^{(k_l)}\right] &= \underbrace{\left(\alpha^{k_l}\right)^4 \left[B_{1\ m\neq 0\&n\neq 0}^{TE_{m,n}}\right] + \alpha^{k_l}\left[B_{1\ m\neq 0}^{TE_{m,0}}\right]}_{\left[B_1^{TE^{(k_l)}}\right]} + \left[B_1^{TM}\right] \\ &= \left[B_1^{TE^{(k_l)}}\right] + \left[B_1^{TM}\right] \end{aligned} \quad (11)$$

Since $\alpha < 1$, when k_l tends toward infinity ($k_l \to +\infty$), the matrix $[B_1^{TE^{(k_l)}}]$ converges to zero. Moreover, for small values of $k_l(1, 2\ldots)$, Fig. 4 and Fig. 5 show a comparison between $[B_1^{TE^{(k_l)}}]$ (for various values of k_l) and $[B_1^{TM}]$ respectively. It is obvious that the contribution of TE modes is negligible compared to that of TM modes.

Thus, for any value of k_l, $[B_1^{(k_l)}]$ is assumed to be independent of the scale level k_l (12).

$$\left[B_1^{(k_l)}\right] = \left[B_1^{TM}\right] = [B_1] \quad (12)$$

Detailed expression of $[B_2^{(k_l,k_l+1)}]$

The impedance operator $\hat{Z}_{k_l+1}$ relative to the previous scale level (k_l+1) is defined on domains (1) and (2) shown in Fig. 2(a) and is expressed by (13). The functions $(f_{n_{active},k_l+1}^{(t)})_{(t=1,2),(n_{active}\in[0,N-1])}$ are the active modes used as excitation sources of scale level (k_l+1).

$$\begin{aligned}\hat{Z}_{k_l+1} &= \hat{Z}_{k_l+1}^{(1)} + \hat{Z}_{k_l+1}^{(2)} \\ \hat{Z}_{k_l+1}^{(1)} &= \sum_{i_{active}} \sum_{j_{active}} \left|f_{i_{active},k_l+1}^{(1)}\right\rangle Z_{k_1+1}(i_{active}, j_{active}) \left\langle f_{j_{active},k_l+1}^{(1)}\right| \\ \hat{Z}_{k_l+1}^{(2)} &= \sum_{i_{active}} \sum_{j_{active}} \left|f_{i_{active},k_l+1}^{(2)}\right\rangle Z_{k_1+1}(i_{active}, j_{active}) \left\langle f_{j_{active},k_l+1}^{(2)}\right| \end{aligned} \quad (13)$$

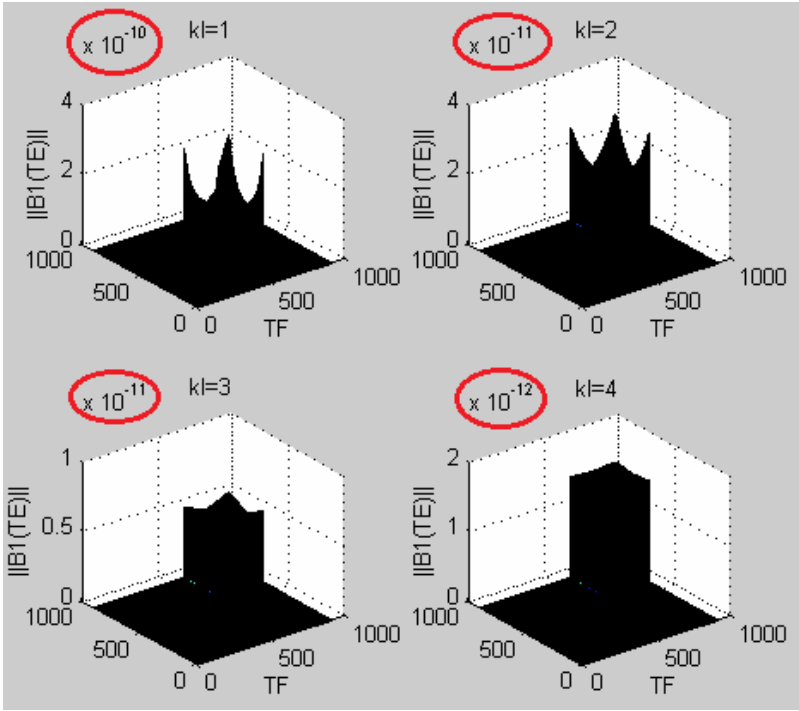

Figure 4. Contribution of the matrix $[B_1^{TE^{(k_l)}}]$ relating to TE modes in the matrix $[B_1^{(k_l)}]$, (TF: number of test functions), the scale level $k_l \in \{1, 2, 3, 4\}$, $||B_1(TE)||$ is the module of each element in the matrix $[B_1^{TE^{(k_l)}}]$. $a = 10.2\,\text{mm}$, $b = 22.9\,\text{mm}$, $w = 0.5\,\text{mm}$, $\alpha = \frac{1}{3}$, $f = 2.45\,\text{GHz}$.

A detailed computation of $[B_2^{(k_l,k_l+1)}]$ leads to the expression (14).

$$\left[B_2^{(k_l,k_l+1)}\right] = \left[B_2\left(\alpha^{k_l+1}\left[Z_{k_l+1}\right]\right)\right] \tag{14}$$

Detailed expression of $[B_{3D}^{(k_l)}]$

The matrix $[B_{3D}^{(k_l)}]$ is due to the surface impedance ZD_{k_l} representing the PIN diode. Using the expression (2) of ZD_{k_l} and the testing functions (Appendix A), we demonstrate that the matrix $[B_{3D}^{(k_l)}]$ is constant (15).

$$\left[B_{3D}^{(k_l)}\right] = [B_{3D}] \tag{15}$$

When replacing (9), (12), (14) and (15) into Equation (8), an explicit

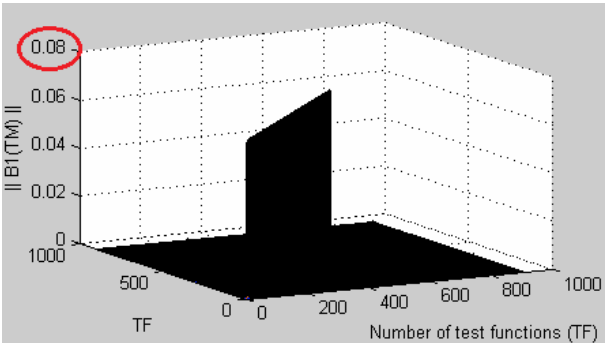

Figure 5. Contribution of the matrix $[B_1^{TM}]$ relating to TM modes in the matrix $[B_1^{(k_l)}]$, $||B_1(TM)||$ is the module of each element in the matrix $[B_1^{TM^{(k_l)}}]$, $a = 10.2\,\text{mm}$, $b = 22.9\,\text{mm}$, $w = 0.5\,\text{mm}$, $\alpha = \frac{1}{3}$, $f = 2.45\,\text{GHz}$.

relation between $[Z_{k_l}]$ and $[Z_{k_l+1}]$ is generated as stated (16).

$$\alpha^{k_l}[Z_{k_l}] = \left(\frac{1}{2}\right)\left([A]\left[[B_1] + \left[B_2\left(\alpha^{k_l+1}[Z_{k_l+1}]\right)\right] + [B_{3D}]\right]^{-1}[A]^T\right)^{-1} \quad (16)$$

3.2.2. Derivation of the Renormalisation Group

Once the explicit relation between $[Z_{k_l}]$ and $[Z_{k_l+1}]$ is defined, the next step is to write this relation in a dimensionless form. This is made possible by replacing the real parameter $[Z_{k_l}]$ by an effective (or renormalized) parameter [10].

In our case, the effective parameter is $[Z'_{k_l}] = \alpha^{k_l}[Z_{k_l}]$. Consequently, the Equation (16) becomes as stated in (17). This equation is called the renormalization group.

$$[Z'_{k_l}] = \left(\frac{1}{2}\right)\left([A]\left[[B_1] + \left[B_2\left([Z'_{k_l+1}]\right)\right] + [B_{3D}]\right]^{-1}[A]^T\right)^{-1} \quad (17)$$

When the iteration of fractal increases infinitely, the input impedance matrix of the infinite fractal structure converges to the fixed point of the renormalization group.

3.2.3. Computation of the Fixed Point

The fixed point characterizes the invariance property of the considered problem. For that, we should find the matrix $[Z]$ verifying the

invariance Equation (18).

$$[Z] = \left(\frac{1}{2}\right)\left([A]\left[[B_1] + [B_2([Z])] + [B_{3D}]\right]^{-1}[A]^T\right)^{-1} \tag{18}$$

To compute $[Z]$, the Equation (18) is expressed as a numerical series M (19). The solution has to be independent of the initial value.

$$M : \begin{cases} Z_0 : \quad \textit{initial value} \\ Z_{n+1} = \left(\frac{1}{2}\right)\left([A]\left([B_1] + [B_2(Z_n)] + [B_{3D}]\right)^{-1}[A]^T\right)^{-1} \end{cases} \tag{19}$$

The algorithm used to determine the fixed point is the following:

1. Start with any initial matrix and fix a tolerated error. The error is defined by $\xi = 100\frac{|\|Z_{n+1}\| - \|Z_n\||}{\|Z_{n+1}\|}(\%)$ and the tolerated error is $\xi_{tolerated} = 0.1\%$.
2. Compute $Z_1 = M(Z_0)$ and fix $n = 1$ (n will be used to compute the number of iterations needed to compute the fixed point).
3. While $(\xi > \xi_{tolerated})$ do
$$Z_{n+1} = M(Z_n);$$
$$n \leftarrow n + 1;$$
End
4. The fixed point is Z_{n+1}.

4. NUMERICAL RESULTS

The purpose of this work is to compute the input impedance of the infinite fractal structure shown Fig. 1. For that, we have used an improved version of the MS-GEC method thanks to RGT concepts. The solution is the fixed point of the renormalization group.

4.1. Computation of the Fixed Point

In a previous paper [8], it was demonstrated that the MS-GEC method converges toward the MoM method when a sufficient number of active modes is used (more than 20 active modes). For that, we choose to excite all the scale levels by 28 active modes. Therefore, the fixed point is a (28×28) matrix. To compute it, we choose to start with a null initial value (20a). At convergence, the residual error ξ relating to each element of the fixed point is depicted in Fig. 6. It is clear that the residual error is less than the tolerated error (0.1%).

To prove that the fixed point is independent of the initial value, we repeat the computation of the fixed point starting with another initial

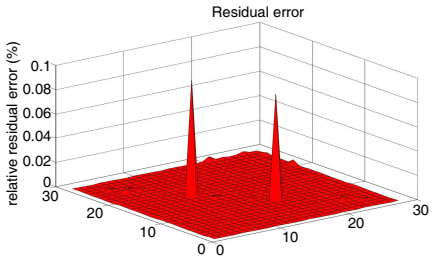

Figure 6. Residual error variation proving the convergence to the fixed point ($\xi_{tolerated} = 0.1\%$), $a = 10.2\,\text{mm}$, $b = 22.9\,\text{mm}$, $w = 0.5\,\text{mm}$, $\alpha = \frac{1}{3}$, $f = 2.45\,\text{GHz}$.

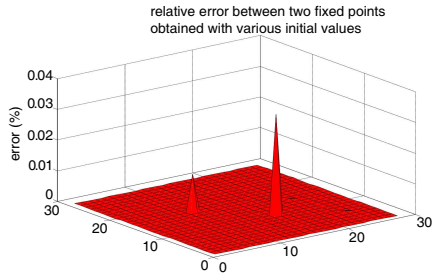

Figure 7. Relative error between two fixed points obtained using two different initial values, $a = 10.2\,\text{mm}$, $b = 22.9\,\text{mm}$, $w = 0.5\,\text{mm}$, $\alpha = \frac{1}{3}$, $f = 2.45\,\text{GHz}$.

value (20b). The relative error between the two fixed points computed using two different initial values is less than 0.04% (Fig. 7).

Physically, the initial value can be viewed as the input impedance of the intermediate scale level from which we start computing the input impedance of the infinite fractal structure. The independency from the initial value means that, starting from any scale level, the input impedance of the infinite fractal structure (which is the fixed point) is not altered.

$$Z_0 = \begin{bmatrix} 0 & 0 & \dots & 0 \\ 0 & \ddots & \ddots & \vdots \\ \vdots & \ddots & \ddots & 0 \\ 0 & \dots & 0 & 0 \end{bmatrix} \quad (20a), \qquad Z_0 = \begin{bmatrix} i & i & \dots & i \\ i & \ddots & \ddots & \vdots \\ \vdots & \ddots & \ddots & i \\ i & \dots & i & i \end{bmatrix} \quad (20b) \qquad (20)$$

4.2. Validation of the Fixed Point

To prove that the computed fixed point is really the input impedance of the infinite active fractal structure, we go through the following steps:

1. Compute the input impedance matrix for various iteration of fractal (k) to approximate the iteration ($k = k_{\text{approximated\_infinity}}$) of the infinite fractal structure. Thus, $Z_{k_{\text{approximated\_infinity}}}$ is the input impedance of the infinite fractal structure (Z_∞).
2. Define the relative error between the fixed point Z_{Fixed_point} and the input impedance Z_k of various iteration order to demonstrate that Z_k converges toward Z_{Fixed_point} when k increases.

3. Compare the value of the fixed point Z_{Fixed_point} with the input impedance of the approximated infinite fractal structure $Z_{k_{\text{approximated\_infinity}}}$ to prove that the computed fixed point is the input impedance Z_∞ of the infinite fractal structure.

The input impedance matrix of the considered fractal structure at any iteration k is a (28×28) matrix since we choose to excite every scale level by 28 active modes. To determine the iteration order $k_{\text{approximated\_infinity}}$ for which the fractal structure is assumed at infinite, the input impedance is computed for various iteration orders k. Fig. 8 shows the variation of some elements of the input impedance matrix Z_k for $k \in [4, 26]$. It is obvious that starting from the iteration order $k = 16$, we can assume that $Z_{k\geq 16}$ is the input impedance of the infinite fractal structure. Therefore, $Z_\infty = Z_{k_{\text{approximated\_infinity}}} \cong Z_{k\geq 16}$.

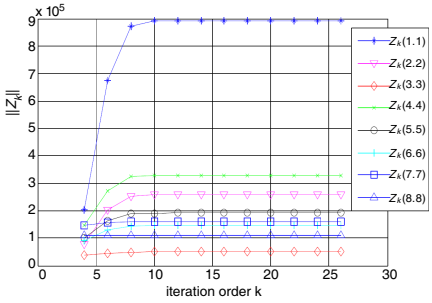

Figure 8. Variation of some elements of the input impedance matrix Z_k with the iteration order k, $a = 10.2\,\text{mm}$, $b = 22.9\,\text{mm}$, $w = 0.5\,\text{mm}$, $\alpha = \frac{1}{3}$, $f = 2.45\,\text{GHz}$.

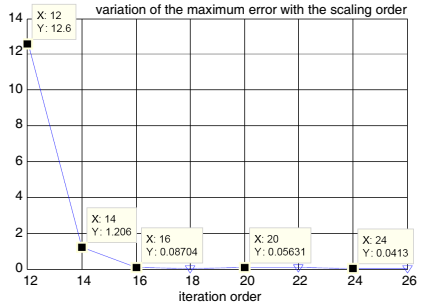

Figure 9. Representation of the maximum error between Z_k and Z_{Fixed_point} for various values of the iteration order k, $a = 10.2\,\text{mm}$, $b = 22,9\,\text{mm}$, $w = 0.5\,\text{mm}$, $\alpha = \frac{1}{3}$, $f = 2.45\,\text{GHz}$.

According to RGT concepts, when the iteration order increases, the input impedance Z_k approaches the fixed point Z_{Fixed_point}. To prove this, we investigated the relative error variation between Z_{Fixed_point} and $(Z_k)_{k\in[12,26]}$. For that, the error made on each element of the input impedance matrix is computed and then the maximum error is selected. Fig. 9 shows the variation of these maximum errors with the iteration order k. Based on the results depicted in Fig. 9, we deduce that starting from the iteration order $(k = 20)$, the fractal structure is at infinite scale. Moreover, the fixed point is proved to be the input impedance of the infinite fractal structure: $Z_{Fixed\_point} = Z_\infty = Z_{k=20}$. Fig. 10 shows the relative error variation between Z_{Fixed_point} and $Z_{k=20}$. The error remains less than 0.06%.

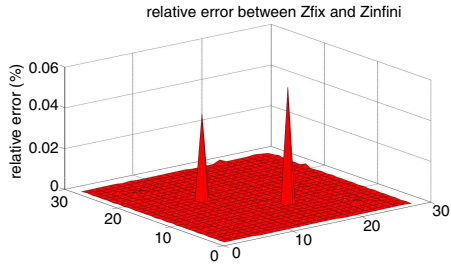

Figure 10. Relative error between the fixed point Z_{Fixed_point} and the input impedance of the infinite fractal structure $Z_{\infty} \cong Z_{k=20}$, $a = 10.2\,\text{mm}$, $b = 22.9\,\text{mm}$, $w = 0.5\,\text{mm}$, $\alpha = \frac{1}{3}$, $f = 2.45\,\text{GHz}$.

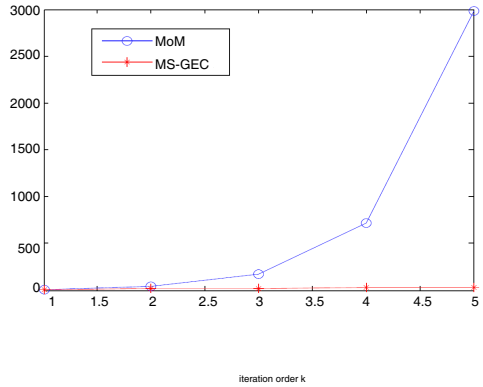

Figure 11. Variation of the processing time with the iteration of fractal [8].

5. ADVANTAGES OF THE MS-GEC COMBINED TO THE RGT

The MS-GEC is a powerful technique appropriate to study fractal-shaped structures since it guarantees an important gain in term of CPU time and memory resources. In fact, the authors had presented in [8] a detailed comparison between (processing time, memory requirement) needed by the MS-GEC method and by the classical Moment method (MoM). It was proved as depicted in Fig. 11 that the processing time varies exponentially with the iteration order when using the MoM method while it varies linearly with the iteration order when using the MS-GEC method. Moreover, since MS-GEC treats the problem in steps, the manipulated matrices at each step have significantly reduced

sizes [8].

However, infinite fractal structures can be studied neither by the MS-GEC nor by any other existing method due to the unknown number of scale levels composing such structures.

The renormalization group theory (RGT) provides an efficient manner which removes the unknown parameter (number of scale levels) from the theory enabling then the study of infinite fractal structures without needing to know the number of scale levels composing it.

6. CONCLUSION

Infinite fractal structures are characterized by their infinite complexity and the unknown number of scale levels composing them. Consequently, their study could not be performed by any of the existing methods who rapidly reach their limits after a limited number of iterations due to the prohibitive increase of CPU time and memory resources required.

Concerning the MS-GEC method, it cannot be applied to infinite fractal structures since the starting elementary scale level cannot be defined.

In this paper, we developed a method which provides an efficient manner to deal with infinite fractal structures. It is called MS-RGT and consists of an extended version of the MS-GEC method thanks to the use of the renormalization group theory (RGT) concepts.

Its main idea is to rewrite the relation between the input impedances of two consecutive scale levels in a dimensionless form by using renormalized parameters. The relation obtained is called renormalization group. Its fixed point is the input impedance of the infinite fractal structure.

The MS-RGT approach is a very powerful technique since it profits from the advantages (rapidity and reduced memory requirements) of the MS-GEC technique and the ability of the RGT to solve problems at their critical point. Its accuracy comes from that of the MS-GEC method which has been demonstrated in the previous paper [8] by a comparison with the widely used Moment method.

APPENDIX A.

The structure at scale level k_l is depicted (Fig. A1). The modal basis $(f_{m,n}^{(k_l)})$, the excitation sources $(f_i^{(k_l)})_{i\in[0,N-1]}$ and the trial functions $(g_p^{(k_l)})$ used to study the scale level k_l are detailed.

A.1. Definition of the Modal Basis

The waveguide enclosing the k_lth scale level is an EMEM waveguide. The modal basis is composed of the modes defined in (A1).

$$
\begin{aligned}
&TE^{(k_l)}_{\substack{m,n \\ m\neq 0 \& n\neq 0}} \\
&= \left| \begin{array}{l}
\dfrac{\frac{n}{\alpha^{k_l}b}}{\sqrt{\left(\frac{m}{a}\right)^2+\left(\frac{n}{\alpha^{k_l}b}\right)^2}} \sqrt{\dfrac{4}{a\alpha^{k_l}b}} \sin\left(\frac{m\pi}{a}\left(x+\frac{a}{2}\right)\right) \sin\left(\frac{n\pi}{\alpha^{k_l}b}\left(y+\frac{\alpha^{k_l}b}{2}\right)\right) \\
\dfrac{\frac{m}{a}}{\sqrt{\left(\frac{m}{a}\right)^2+\left(\frac{n}{\alpha^{k_l}b}\right)^2}} \sqrt{\dfrac{4}{a\alpha^{k_l}b}} \cos\left(\frac{m\pi}{a}\left(x+\frac{a}{2}\right)\right) \cos\left(\frac{n\pi}{\alpha^{k_l}b}\left(y+\frac{\alpha^{k_l}b}{2}\right)\right)
\end{array} \right| \\
&TM^{(k_l)}_{\substack{m,n \\ m\neq 0 \& n\neq 0}} \\
&= \left| \begin{array}{l}
\dfrac{\frac{m}{a}}{\sqrt{\left(\frac{m}{a}\right)^2+\left(\frac{n}{\alpha^{k_l}b}\right)^2}} \sqrt{\dfrac{4}{a\alpha^{k_l}b}} \sin\left(\frac{m\pi}{a}\left(x+\frac{a}{2}\right)\right) \sin\left(\frac{n\pi}{\alpha^{k_l}b}\left(y+\frac{\alpha^{k_l}b}{2}\right)\right) \\
\dfrac{-\frac{n}{\alpha^{k_l}b}}{\sqrt{\left(\frac{m}{a}\right)^2+\left(\frac{n}{\alpha^{k_l}b}\right)^2}} \sqrt{\dfrac{4}{a\alpha^{k_l}b}} \cos\left(\frac{m\pi}{a}\left(x+\frac{a}{2}\right)\right) \cos\left(\frac{n\pi}{\alpha^{k_l}b}\left(y+\frac{\alpha^{k_l}b}{2}\right)\right)
\end{array} \right| \\
&TE^{(k_l)}_{\substack{m0 \\ m\neq 0}} = \left| \begin{array}{l} 0 \\ \sqrt{\dfrac{2}{a\alpha^{k_l}b}} \cos\left(\frac{m\pi}{a}\left(x+\frac{a}{2}\right)\right) \end{array} \right| \\
&TE^{(k_l)}_{\substack{0n \\ n\neq 0}} = \left| \begin{array}{l} 0 \\ -\sqrt{\dfrac{2}{a\alpha^{k_l}b}} \cos\left(\frac{n\pi}{\alpha^{k_l}b}\left(y+\frac{\alpha^{k_l}b}{2}\right)\right) \end{array} \right| \\
&TEM^{(k_l)} = \left| \begin{array}{l} 0 \\ \sqrt{\dfrac{1}{a\alpha^{k_l}b}} \end{array} \right|
\end{aligned}
\tag{A1}
$$

A.2. Choice of Active Modes

The active modes used as artificial excitation sources are chosen among the modes of the modal basis (A1). The first active mode is the $TEM^{(k_l)}$; it is a propagating mode since its cutoff frequency is null.

The other active modes are chosen among the $TM^{(k_l)}_{0n}$ modes. These latter should respect the structure symmetry with regard to its symmetry plan ($y = 0$). Consequently, only $(TM^{(k_l)}_{0(2n)})_{n\in[1\,,\,N-1]}$ are used as active modes.

A.3. Choice of Test Functions

The virtual current is defined on the impedance operator domains and on the diode domain, it is null elsewhere. The

current is expressed as the sum of known test functions $\{(g_p^{(k_l)})_{\hat{Z}_{k_l+1}\ domains}, (g_{p,ZD}^{(k_l)})_{ZD_{k_l}domain}\}$ weighted by unknown coefficients $\{(x_p^{(k_l)}), (x_{p,ZD}^{(k_l)})\}$.

In this work, we used piecewise linear [20] test functions (Fig. A1) having the same vertical polarization as the excitations sources. Their expressions on $\hat{Z}_{k_l+1}$ and ZD_{k_l} domains are expressed by (A2) and (A3) respectively.

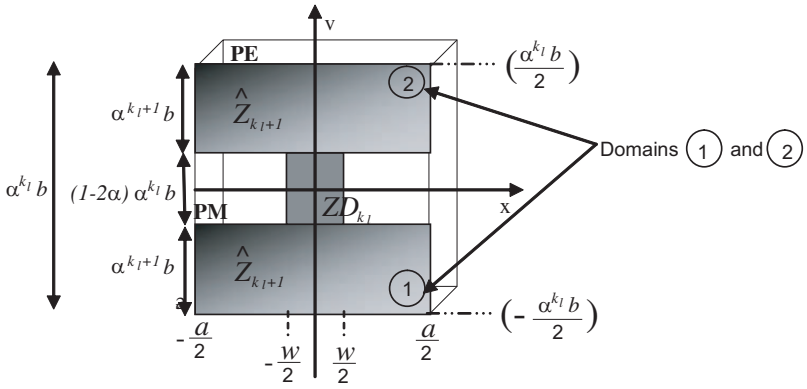

Figure A1. Detailed description of the structure at the k_lth scale level.

To avoid the errors due to the discontinuities between domains when computing the current, the concept of attachment functions was introduced. At each interface, one attachment function is used.

$$g_p^{(k_l)}(x,y) = \begin{cases} 0 \\ \left\{ \begin{array}{ll} \dfrac{\Delta y_{k_l} - \left| y - y_p^{(k_l)} \right|}{\Delta y_{k_l}} & \text{if} \quad y \in \left[y_{p-1}^{(k_l)}, y_{p+1}^{(k_l)} \right],\ x \in \left[-\frac{a}{2},\ \frac{a}{2} \right] \\ 0 & \text{otherwise} \end{array} \right. \end{cases} \tag{A2}$$

$$g_{p,ZD}^{(k_l)}(x,y) = \begin{cases} 0 \\ \left\{ \begin{array}{ll} \dfrac{\Delta y_{ZD,k_l} - \left| y - y_{p,ZD}^{(k_l)} \right|}{\Delta y_{ZD,k_l}} & \text{if} \quad y \in \left[y_{p-1,ZD}^{(k_l)}, y_{p+1,ZD}^{(k_l)} \right],\ x \in \left[-\frac{w}{2},\ \frac{w}{2} \right] \\ 0 & \text{otherwise} \end{array} \right. \end{cases} \tag{A3}$$

where

$$\Delta y_{k_l} = \frac{\alpha^{k_l+1} b}{2(Ny+1)}, \quad \Delta y_{ZD,k_l} = \frac{(1-2\alpha)\alpha^{k_l} b}{2(Ny_D+1)}$$

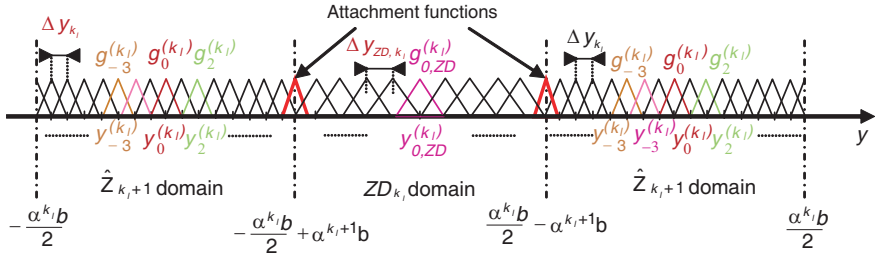

Figure A2. Representation of the attachment functions and the piecewise linear functions used as test functions.

REFERENCES

1. Mandelbrot, B., *Les Objets Fractals*, 4th edition, Flammarion, 1995.
2. Werner, D. H. and R. Mittra, *Frontiers in Electromagnetics*, IEEE Press, NJ, 2000.
3. Skrivervik, A. K., J. F. Zurcher, O. Staub, and J. R. Mosig, "CS antenna design: The challenge of miniaturization," *IEEE Transactions on Antennas and Propagation*, Vol. 43, No. 4, 12–27, August 2001.
4. Gianvittono, J. and Y. Rahmat Samii, "Fractal antennas: A novel antenna miniaturization technique and applications," *IEEE Antennas Propag. Mag.*, Vol. 44, No. 1, 20–36, 2002.
5. Tennant, A. and B. Chambers, "A single-layer tuneable microwave absorber using an active FSS," *IEEE Microwave and Wireless Components Letters*, Vol. 14, No. 1, 46–47, January 2004.
6. Chang, K., S. I. Kwak, and Y, J. Yoon, "Equivalent circuit modeling of active frequency selective surfaces," *IEEE Radio and Wireless Symposium*, 663–666, 2008.
7. Bossard, J. A., D. H. Werner, T. S. Mayer, and R. P. Drupp, "A novel design methodology for reconfigurable frequency selective surfaces using Genetic Algorithms," *IEEE Transactions on Antennas and Propagation*, Vol. 53, No. 4, 1390–1400, April 2005.
8. Mili, S., C. Larbi Aguili, and T. Aguili, "Study of fractal-shaped structures with pin diodes using the multi-scale method combined to the generalized equivalent circuit modeling," *Progress In Electromagnetics Research B*, Vol. 27, 213–233, 2011.
9. Wilson, K. G., "The renormalization group and critical phenomena," *Nobel Lecture*, December 8, 1982.

10. Fisher, M. E., "Renormalization group theory: Its basis and formulation in statistical physics," *Reviews of Modern Physics*, Vol. 70, No. 2, April 1998.
11. Wilson, K. G. and J. Kogut, "The renormalization group and the ε expansion," *Physics Reports (Section C of Physics Letters)*, Vol. 12, No. 2, 75–200, 1974.
12. Wilson, K. G., "Renormalisation group and Kadanoff Scaling picture," *Physics Rev. B*, Vol. 4, 3174, 1971.
13. Fisher, M. E., "The renormalization group and the theory of critical behaviour," *Reviews of Modern Physics*, Vol. 46, 597, April 1998.
14. Pelissetto, A. and E. Vicari, "Critical phenomena and renormalization group theory," *Physics Reports*, April 2002.
15. Larbi Aguili, C., A. Bouallegue, and H. Baudrand, "Utilisation d'un processus de renormalisation pour l'étude électromagnétique des structures fractales bidimensionnelles," *Annales des Télecommunications*, Vol. 60, Nos. 7–8, 1023–1050, Juillet-Août, 2005.
16. Aguili, T., "Modélisation des composants S.H.F planaires par la méthode des circuits équivalents généralisés," Thesis, National Engineering school of Tunis ENIT, May 2000.
17. Baudrand, H., "Representation by equivalent circuit of the integral methods in microwave passive elements," *European Microwave Conference*, Vol. 2, 1359–1364, Budapest, Hungary, September 10–13, 1990.
18. Baudrand, H. and H. Aubert, *L'Electromagnétisme par les Schémas Equivalents*, Cepaduès Éditions, 2003.
19. Kiani, G. I., K. P. Esselle, A. R. Weily, and K. L. Ford, "Active frequency selective surface using PIN diodes," *Antennas and Propagation Society International Symposium*, 4525–4528, Honolulu, HI, June 9–17, 2007.
20. Wilton, D. R. and C. M. Butler, "Efficient numerical techniques for solving pocklington's equation and their relationship to other methods," *IEEE Transactions on Antennas and Propagation*, 83–86, January 1976.